Bulletin of the Seismological Society of America, Vol. 105, No. 3, pp. –, June 2015, doi: 10.1785/0120140302

A Monte Carlo Method for Probabilistic Hazard Assessment of Induced Seismicity due to Conventional Natural Gas Production

by S. J. Bourne, S. J. Oates, J. J. Bommer, B. Dost, J. van Elk, and D. Doornhof

Abstract A Monte Carlo approach to probabilistic seismic-hazard analysis is developed for a case of induced seismicity associated with a compacting gas reservoir. The geomechanical foundation for the method is the work of Kostrov (1974) and McGarr (1976) linking total strain to summed seismic moment in an earthquake catalog. Our Monte Carlo method simulates future seismic hazard consistent with historical seismic and compaction datasets by sampling probability distributions for total seismic moment, event locations and magnitudes, and resulting ground motions. Ground motions are aggregated over an ensemble of simulated catalogs to give a probabilistic representation of the ground-motion hazard. This approach is particularly well suited to the specific nature of the time-dependent induced seismicity considered.

We demonstrate the method by applying it to seismicity induced by reservoir compaction following gas production from the Groningen gas field. A new ground-motion prediction equation (GMPE) tailored to the Groningen field has been derived by calibrating an existing GMPE with local strong-motion data. For 2013–2023, we find a 2% chance of exceeding a peak ground acceleration of 0.57g and a 2% chance of exceeding a peak ground velocity of 22 cm/s above the area of maximum compaction. Disaggregation shows that earthquakes of M_w 4–5, at the shortest hypocentral distances of 3 km, and ground motions two standard deviations above the median make the largest contributions to this hazard. Uncertainty in the hazard is primarily due to uncertainty about the future fraction of induced strains that will be seismogenic and how ground motion and its variability will scale to larger magnitudes.

Introduction

Several energy technologies have been observed to have the potential for causing induced earthquakes (e.g., Majer *et al.*, 2007; Suckale, 2009; Evans *et al.*, 2012; Davies *et al.*, 2013; Ellsworth, 2013; International Energy Agency Environmental Projects Ltd., 2013; Klose, 2013; National Academy of Sciences, 2013), and in recent years public awareness and concern regarding the possible impacts of such events has grown. Operators and regulators alike need to make risk-informed decisions for the management of the threat that may be posed by such projects, in which risk may be thought of as the product of hazard, exposure, and vulnerability. Seismic-hazard assessments are essential to inform the choice of any risk mitigation options.

The design and implementation of any risk mitigation measures necessarily must begin with a quantification of the ground-shaking hazard due to induced seismicity. The well-established approaches used to analyze ground-shaking hazard due to natural seismicity cannot be directly applied to induced earthquakes. The main challenge lies in the fact that induced seismicity, unlike natural tectonic earthquake activity, cannot be treated as stationary in time, which is a standard assumption in probabilistic seismic-hazard analysis (PSHA). Time-dependent PSHA models have been developed but these are usually based on short-term probabilities of events considering the current position in the seismic cycle (e.g., Petersen *et al.*, 2007; Akinci *et al.*, 2009) or the effects of Coulomb stress transfer following large earthquakes (e.g., Parsons *et al.*, 2000). The problem of induced seismicity, in which the recurrence characteristics may increase significantly over a short period of time (and then possibly recede to background levels in the longer term), requires the development of different approaches. Additionally, the models developed need to accommodate earthquakes over magnitude ranges that are quite different (i.e., much smaller values) than those considered in PSHA for natural seismicity, and the fact that these will generally occur at very shallow depths.

Responding to the growing public and regulatory concerns about induced seismicity, hazard assessment approaches have been developed in recent years, particularly for enhanced geothermal systems (Convertito *et al.*, 2012; Mena *et al.*, 2013). Because the mechanism by which induced earthquakes are caused by energy production or waste

disposal activities vary appreciably from one technology to another (Ellsworth, 2013), approaches need to be developed for specific applications. In this article, we first briefly review the existing methods of seismic-hazard assessment and then present a Monte Carlo seismic-hazard model based on a time-dependent stochastic seismological model for earthquakes induced by conventional gas production (Bourne *et al.*, 2014). This model is then illustrated with application to the Groningen gas field in The Netherlands, but its key elements may be adaptable to other gas fields. The approach may also be a useful option for those dealing with the assessment of seismic hazard from induced earthquakes in general.

Methods of Seismic-Hazard Assessment

The two essential elements of a seismic-hazard assessment are a model for the location and magnitude of possible future earthquakes, and a model to estimate the ground motions on a site with specified near-surface characteristics at a given distance from an earthquake of specified magnitude. The combination of these two models results in an estimate of the resulting ground motion at a site of interest. In effect, PSHA treats both the location and frequency of future earthquakes of different magnitudes as aleatory (random) distributions. The same is true for the variability in predicted ground motions from each earthquake, represented by the logarithmic standard deviation of the residuals, which is generally referred to as sigma (e.g., Strasser *et al.*, 2009). In PSHA, one integrates over these distributions to calculate the rate at which ground-motion levels are exceeded as a result of all possible earthquakes.

The framework for PSHA was originally proposed by Cornell (1968) and then underwent additional development during subsequent years (McGuire, 2008). The primary output for each ground-motion parameter considered is a hazard curve showing the annual frequency of different levels of this parameter. The process can also be inverted to identify the magnitude–distances bins contributing most strongly to the hazard associated with a given ground-motion parameter at a particular annual exceedance frequency; this is referred to as disaggregation or deaggregation (McGuire, 1995; Bazzurro and Cornell, 1999).

An alternative to integrating over the distributions of magnitude, distance, and ground-motion variability (specified by epsilon, ϵ, the number of standard deviations away from the logarithmic mean value) is to sample them using Monte Carlo simulations. Monte Carlo approaches to PSHA are well established (Ebel and Kafka, 1999; Musson, 1999, 2000; Assatourians and Atkinson, 2013; Pagani *et al.*, 2014), although they are not as widely used in practice as the classical approach of direct numerical integration, possibly because they can be computationally demanding when hazard estimates are required at low annual frequencies of exceedance.

Seismic risk, in terms of the probability of a particular consequence, at a single location can be calculated through the convolution of a hazard curve with a fragility curve quantifying the probability of a given consequence occurring under different levels of ground shaking. To apply the same approach to a geographically distributed exposure (such as the building stock in a given region) by first calculating hazard curves at multiple locations using conventional PSHA, leads to overestimation of the aggregated damage or losses (Crowley and Bommer, 2006). The reason for this lies in the nature of the ground-motion variability (sigma), which is a major contributor to the hazard estimates. The total variability can be decomposed into between-event and within-event components, the former representing earthquake-to-earthquake variability and the latter the record-to-record variability (e.g., Al Atik *et al.*, 2010). The between-event variability reflects the influence of source parameters not generally included in the ground-motion prediction equations (GMPEs) such as stress drop and slip distribution on the fault. The within-event variability reflects the difference in travel paths and site response characteristics among sites with the same time-averaged shear-wave velocity in the top 30 m (V_{S30}) and the influence of the deeper geological structure. The within-event component of the variability is generally much larger than the between-event component. Conventional PSHA does not distinguish between the two components of variability hence parallel calculations for multiple sites effectively treats all of the variability as being between-event sigma.

To avoid the problems associated from misrepresentation of the ground-motion variability arising from applying conventional PSHA at multiple locations simultaneously, one may calculate the risk by generating ground-motion fields for each event in a synthetic earthquake catalog and convolving these motions with the fragility functions to develop statistics of damage or loss. Using Monte Carlo simulations, a value of the between-event variability can be sampled for each earthquake and then values of the within-event variability are sampled at each location for this event. This will not lead to uniformly high-ground shaking fields because even for a large value of between event there will be great variations in the resulting motions at different sites at the same distance from the earthquake source as a result of the within-event variability.

Monte Carlo Seismic-Hazard Simulation

The simulation method developed for induced seismicity associated with the compaction of a producing gas field is based on the Monte Carlo variant of PSHA. Bourne *et al.* (2014) provide a detailed description of this seismological model.

Simulation Method

Kostrov (1974) provides an equivalence between the average strain due to seismogenic fault slip and the total seismic moment within a given volume and time interval.

Independently, McGarr (1976) obtained the same result for special cases related to subsurface volume changes. Building on these results, we consider the average seismogenic strain to be some fraction of the average total strain, to reflect the possibility that not all strain is accommodated by seismogenic slip on faults. This strain-partitioning fraction is therefore limited to assume values between null and unity and in general may be a function of other variables. Tectonically, triggered seismicity is excluded from the assessed hazard based on the absence of natural seismicity, as revealed by both the historical and instrumental records for this region (Dost and Haak, 2007).

In the particular case of volumetric changes of the Groningen gas reservoir, a suitable parameter for representing variability in strain partitioning is the bulk reservoir volume change per unit area, or the change in bulk reservoir thickness. The functional form of the strain-partitioning function is empirically motivated and taken to be a generalized two-parameter logistic function. This satisfies the requirement for the function to remain between null and unity while matching the observed log–linear trend between strain partitioning and reservoir thickness changes. A standard Monte Carlo procedure yields the set of parameter pairs consistent with these observations. For each pair of acceptable parameters, a total seismic moment may be calculated for a given reservoir compaction model through time according to that particular instance of the strain-partitioning function. Repeating this procedure for every set of acceptable model parameters yields a probability distribution of total seismic moments (Bourne *et al.*, 2014). Through a similar procedure, a relative probability map of event epicenters are equivalent to the normalized seismic moment density maps obtained from the strain-partitioning model (Bourne *et al.*, 2014).

The next step is to simulate a catalog of earthquake locations and magnitudes consistent with the probability distribution of total seismic moment and event epicenters for a given time interval.

1. *Total seismic moment:* Choose a single random independent sample from the total seismic moment distribution.
2. *Location:* Choose a single epicenter at random, weighted by the relative probability map of epicenters. This is achieved by selecting a random location, then selecting a random number to decide if an event occurs at this location according to the relative probability map. This process is repeated until an event location is identified.
3. *Magnitude:* Choose a single random independent event magnitude from the frequency–magnitude distribution. This distribution is truncated on both sides of the distribution. The lower truncation reflects the minimum magnitude to be simulated, M_{min}. In PSHAs conducted to provide input for engineering design for natural earthquakes, this magnitude will reflect the smallest earthquakes considered capable of generating ground motions that could potentially cause damage to engineered structures. Motions from smaller earthquakes, even if of high amplitude, will be of insufficient duration and energy content to pose a threat to well-built structures designed for lateral loading. Values used in practice are usually in the range M_{w} 4–5, but for induced earthquakes—as discussed below—it is appropriate to consider much lower thresholds, while not being so small as to lead to excessive simulation times. The upper truncation is required so there is zero chance the event magnitude exceeds M_{max}. The value of M_{max} used to sample the magnitude of the first event corresponds to the total seismic moment obtained in step 1. Subsequently, M_{max} is lowered by an amount corresponding to the total seismic moment of the events already simulated.
4. *Catalog:* Repeat steps 2 and 3 until the total seismic moment of sampled population is equal to that obtained in step 1 to within some suitably small tolerance.
5. *Ground motion:* For each event in the catalog choose a single random independent value for the event-specific epsilon, which corresponds to the number of standard deviations of the between-event variability. For each observation point at the Earth's surface, choose a single random independent value for the within-event epsilon. For each combination of observation point and event, compute the ground motion according to the selected combination of the between-event and within-event epsilon values.
6. *Hazard:* Count the number of times a given ground-motion threshold is exceeded for each observation point. Repeat this for a range of ground-motion thresholds.
7. *Statistics:* Repeat all steps until the average exceedance rates per catalog are sufficiently free from stochastic error for all surface observation points and ground-motion thresholds of interest.

Ground-Motion Prediction Equations

GMPEs are an indispensable element of any PSHA model. The equations predict a probabilistic distribution, characterized by a median and a standard deviation, of logarithmic values of the selected ground-motion parameter, such as peak ground acceleration (PGA) or peak ground velocity (PGV), as a function of explanatory variables such as magnitude, style-of-faulting, distance, and site characterization. Most empirically derived GMPEs are not immediately applicable to PSHA for induced seismicity because they are obtained from regressions on recordings of earthquakes of M_{w} 4–5 and greater, whereas hazard assessment of induced seismicity may consider much smaller earthquakes. The motions from such earthquakes are not considered to be of engineering significance, as reflected also in the choice of similar values M_{min} in the standard PSHA practice. There are at least three reasons why smaller magnitude earthquakes may be of relevance when dealing with induced rather than natural seismicity:

1. Induced earthquakes will generally occur at shallower depths than natural events, creating shorter travel paths to surface locations;
2. although ground shaking from earthquakes of less than M_{w} 4 may not be of relevance to the design of new struc-

tures, vulnerable existing buildings may be susceptible to such motions; and
3. because the hazard from induced seismicity will often be perceived as an imposed condition, public tolerance to even low shaking levels may be limited.

Selecting appropriate GMPEs for such applications is therefore challenging, and criteria such as those proposed by Bommer *et al.* (2010) are not useful without modification to the specific characteristics of induced seismicity. Special consideration needs to be given, for example, to the distance metric employed in the GMPE. The use of equations based on distances measured horizontally (epicentral R_{epi}, or Joyner–Boore, R_{JB}) would implicitly assume equivalence of focal depth distributions in the host region (for which the equation was derived) and target region (where it is being applied). This is unlikely to be the case if the equation has been derived for natural seismicity. Even for GMPEs using distance metrics that account for depth (hypocentral, R_{hyp}, or rupture distance, R_{rup}), their application to induced earthquakes may extrapolate the equations beyond their strict limits of validity. Moreover, the effect of shallow depths may be partially counteracted by lower stress drop for such shallow earthquakes, leading to potential overestimation of the surface motions. An even more serious issue is that it has been found that the extrapolation of empirical GMPEs to earthquakes of smaller magnitude than the lower limit in the database from which they are derived, generally results in overestimation of the resulting ground motions (Bommer *et al.*, 2007; Atkinson and Morrison, 2009).

An additional complication is that ground motions from smaller magnitude events often reveal regional differences that do not persist at the larger magnitudes considered in conventional PSHA (e.g., Chiou *et al.*, 2010) other than those related to differences in long-distance attenuation and systematic differences in site amplification functions. Therefore, even GMPEs derived for the appropriate magnitude and depth ranges, such as the models recently proposed for induced earthquakes in the Geysers geothermal region by Sharma *et al.* (2013) may not be automatically usable. The suite of stochastic GMPEs derived by Douglas *et al.* (2013) for small-magnitude shallow-focus induced earthquakes associated with geothermal systems would offer a useful option if there was reliable knowledge of the source and path parameters in the target region. For the preliminary hazard model for the Groningen field, in which it was decided to directly predict the ground motions at the surface of soft soil sites, the hard reference rock conditions of the Douglas *et al.* (2013) equations would present a additional challenge.

A further consideration in selecting or developing appropriate GMPEs for this application is that the aleatory variability (sigma) must be decomposed into its between-event and within-event components (e.g., Al Atik *et al.*, 2010) to enable correct sampling in the Monte Carlo simulations, as discussed previously. This is not a particularly strong selection criterion, however, because it has become standard practice to provide the between- and within-event standard deviations.

Application to the Groningen Gas Field

The Groningen field is located in the northeast of The Netherlands (Stauble and Milius, 1970) and is one of the world's 20 largest gas fields. The reservoir is a more than 250 m thick Slochteren sandstone of the Upper Rotliegend Group, at a depth of approximately 3 km. Faults mapped at the base of the Zechstein salt formation, located just above the reservoir, typically strike north-northwest. The field was discovered in 1959 and has been in production since 1963. Some 300 wells have been drilled, spread over 29 production clusters. The recoverable volume of gas is about 2800 billion cubic meters. As of November 2012, about 70% of this original recoverable volume has been produced leaving a further 800 billion cubic meters to be produced over about the next 70 years.

The Royal Netherlands Meteorological Institute (KNMI) has monitored the seismicity in The Netherlands since 1908, and the first earthquake recorded in the north of The Netherlands was in December 1986. Current seismicity observed in this area is generally considered to be induced by production from the northern gas fields, Groningen, and others. A local monitoring network in the northeast of The Netherlands was installed in 1995. This network originally consisted of eight stations at which three-component geophones were deployed at four depth levels in shallow (200–300 m deep) boreholes. In 2010, a major upgrade of this array was carried out. This is composed of expansion of the network by deploying six additional stations (in 120 m deep boreholes), implementation of real-time continuous data transmission to the data center, and an automatic detection and location capability. Complementing the geophone array, a number of accelerometer stations were also added to the network for surface strong-motion measurements which can also be used as an additional input to the event location calculations. Dost *et al.* (2012) describe the composition of the monitoring network and its evolution over time. Figure 1 shows the stations comprising the network in the northern part of The Netherlands which at the time of writing consists of 17 borehole stations and 23 accelerometers (some are outside the coverage of the map).

It is generally accepted that for the Groningen field earthquake catalog, the magnitude of completeness for located events is local magnitude (M_L) 1.5, starting in April 1995, with an event-detection threshold of M_L 1.0 (Dost *et al.*, 2012). Magnitude values are given to the nearest tenth. KNMI (Eck *et al.*, 2006) concludes that M_w and M_L are essentially equivalent in this area over the observed magnitude range. Based on this the two scales are taken to be locally equivalent, but we recognize that may require subsequent revision based on the outcome of ongoing further investigations by KNMI (Dost *et al.*, 2013). According to location residuals, epicenters of events in the catalog are determined to within about 0.5 to 1 km but, because of the sparseness of the monitoring array, depths may only be estimated for a handful of fortuitously positioned events. For other events, a depth of 3 km was assumed corresponding to the average depth of the reservoir.

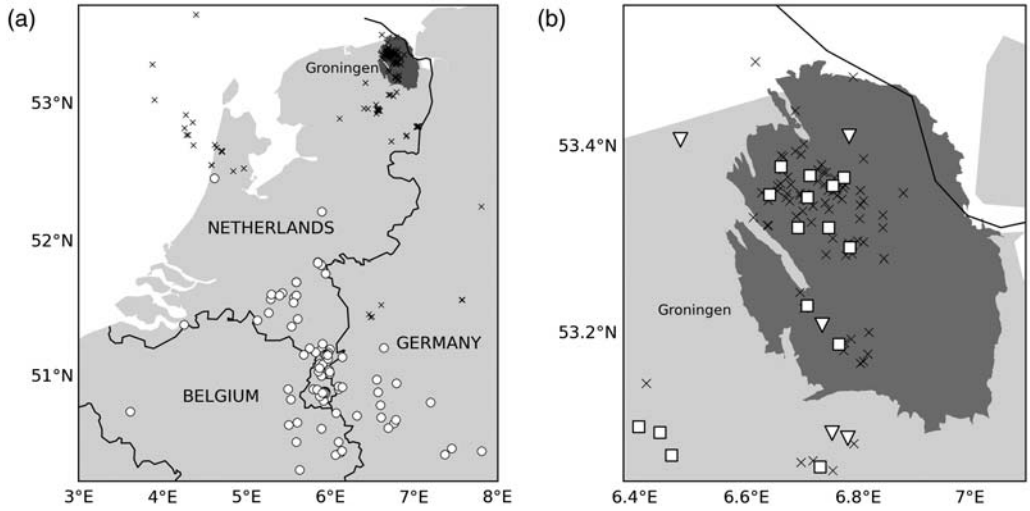

Figure 1. (a) The Groningen gas field is located in the northeast of The Netherlands close to the city of Groningen. The 1987–2013 distribution of $M_L \geq 2$ earthquakes reported by The Royal Netherlands Meteorological Institute (KNMI) indicate induced seismicity (black crosses) linked with onshore and offshore producing gas fields with some natural seismicity further south (white circles). (b) The network of shallow borehole geophones (triangles) and surface accelerometers (squares) used for monitoring earthquakes within the vicinity of the Groningen field.

PSHA were carried out by KNMI using various vintages of the earthquake catalog. A series of publicly available reports and papers (de Crook *et al.*, 1995, 1998; Wassing *et al.*, 2004; Eck *et al.*, 2006; Dost *et al.*, 2012) document this work on monitoring and hazard analysis. The consensus between these numerous studies was that the maximum magnitude earthquake that could be induced by gas production in the north of The Netherlands was $M_{max} \sim 3.9$.

An M_L 3.6 earthquake that occurred on 16 August 2012 near Huizinge, above the central part of the Groningen field, along with concerns that induced seismicity was increasing, motivated efforts to reassess the induced seismic hazard. Three subsequent studies (Dost and Kraaijpoel, 2013; Muntendam-Bos and de Waal, 2013; Bourne *et al.*, 2014), using seismicity data up to the 2012 M_L 3.6 Huizinge event, concluded that the frequency–magnitude distribution of observed earthquakes for the Groningen gas field do not provide any evidence for a reliable upper bound on the maximum magnitude earthquake that Groningen gas production may induce in the future.

For this reason, the previous seismic-hazard assessments must be revised. Moreover, a significant amount of new data has become available since the previous hazard update by KNMI. The report of Dost *et al.* (2012) is based on analysis of the data up to and including 1 January 2010, whereas the major upgrade of the monitoring system was carried out during 2010. Dost *et al.* (2012) reported that the catalog for the north of The Netherlands contained 640 events. In this report, we restrict our analyses to the 187 events with $M_L \geq 1.5$ recorded within the Groningen field between 1 April 1995 and 30 October 2012, the start date being determined by the requirement that the magnitude of completeness must be M_L 1.5 for the whole of the period considered.

An alternative estimate of the maximum magnitude based on releasing all induced strain within a single event yields a value of 6.5 (Bourne *et al.*, 2014). However, we will show that this upper bound does not influence the seismic-hazard assessment.

Seismological Model for Reservoir Compaction

The model of compaction for the Groningen field is based on the distribution of pressure changes represented within a reservoir simulation model that is calibrated to match the history of gas production from each well and the history of pressure depletion and limited aquifer influx witnessed by a network of observation wells. The initial model considered for reservoir compaction in response to these pressure changes is linear elastic, in which compaction is the product of reservoir pressure depletion, net reservoir thickness, and the uniaxial compressibility of the bulk reservoir.

The distribution of net reservoir thickness was taken from a static reservoir model constrained by reflection seismic data and well data. The distribution of uniaxial compressibility depends on reservoir porosity taken from a static reservoir model constrained by petrophysical well logs. The total reservoir pore volume was constrained to match the volume of gas initially in place, obtained from analysis of pressure depletion versus gas production data. However, uncertainty remains in the distribution of porosity, particularly away from well control. The relationship between reservoir porosity and uniaxial compressibility was based on laboratory measurements of plug and core samples recovered from the reservoir. Some uncertainty remains in the relationship between these measurements and the uniaxial compressibility of the bulk reservoir due to limited sampling and differences in length scale. This was represented as a single field-wide scalar parameter which was constrained by minimizing the misfit between the computed surface subsidence

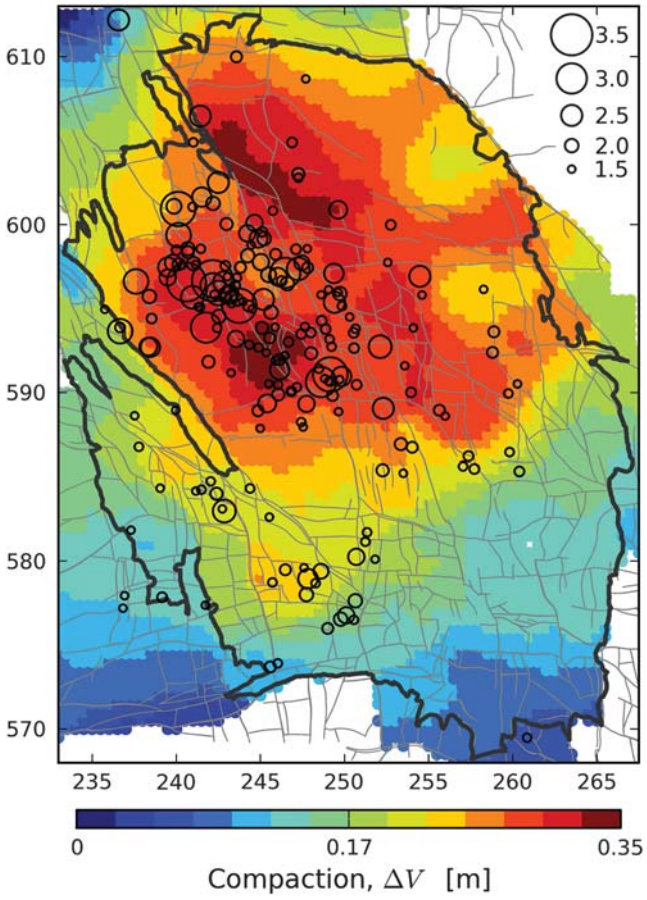

Figure 2. Earthquake epicenters for $M_L \geq 1.5$ from 1995 to 2012 in relation to the model of reservoir compaction from 1960 to 2012. The thick gray polygon denotes the outline of the Groningen field. Thin gray lines denote faults mapped close to the reservoir level. Map coordinates are given as kilometers within the Dutch national triangulation coordinates system (Rijksdriehoek).

and a comprehensive network of geodetic subsidence measurements obtained regularly since 1964 using leveling and Interferometric Synthetic Aperture Radar (InSAR) methods (Bourne *et al.*, 2014).

The resulting linear elastic compaction model (Fig. 2) yields a reasonable fit to these geodetic data. However, there are alternative reservoir compaction models, such as higher-order models for the relationship between reservoir pressure depletion and compaction. One depends on the time history of local pressure depletion. Another depends on the instantaneous local rate and state of pressure depletion. Also there remains uncertainty about the mechanical properties of the subsurface surrounding the reservoir measured from petrophysical logs and core materials. These properties influence the relationship between reservoir compaction and surface subsidence, and so allow another set of alternative compaction models. All these alternative reservoir compaction models are consistent with the available reservoir and geodetic data, but yield different predictions for future reservoir compaction.

Application of the seismological model developed for reservoir compaction to the initial linear-elastic reservoir compaction model and the 2013 plan for future gas production yields a model for the total seismic moment distribution (Fig. 3) and the map distributions of event density (Fig. 4). These exhibit time dependence due to the variation in compaction with time.

GMPE for Induced Earthquakes

An important step in the hazard assessment was to select appropriate ground-motion parameters to characterize the shaking hazard in the Groningen field. The choices for the preliminary studies were PGV, a simple parameter that is considered a reasonable indicator of the damage potential due to ground shaking (e.g., Bommer and Alarcón, 2006), and PGA, because it is still among the parameters most commonly used to characterize building fragility functions (e.g., Bothara *et al.*, 2010).

In view of the issues discussed previously regarding magnitude scaling, focal depths, regional variations in ground motion, and the influence of local site conditions, the obvious choice appeared to be the GMPEs of Dost *et al.* (2004). These equations for PGA and PGV were derived using recordings on soft soil sites of small-magnitude, shallow-focus induced earthquakes in The Netherlands, which suggests an almost perfect match to the target requirements. Two limitations of the Dost *et al.* (2004) model are that it provides only a total sigma, although a decomposition into within- and between-event elements could be assumed, and that by modeling a linear scaling with magnitude it is likely to yield grossly overestimated predictions for larger magnitudes. In fact, comparisons of the predictions from the Dost *et al.* (2004) equation with 40 recordings (obtained at epicentral distances up to 13 km from eight induced earthquakes of M_w 2.7 to 3.6) in the Groningen field revealed very significant overestimation (Fig. 5). The data used by Dost *et al.* (2004) were predominantly from the Roswinkel gas field with no recordings from Groningen. A possible explanation for the apparently very large difference in the surface motions in these two locations is the presence of a high-velocity layer (Zechstein salt formation) immediately above the gas reservoir in the Groningen field, which could act as a barrier reflecting and refracting a large part of the seismic energy; in the Roswinkel field, the Zechstein formation is below the seismicity within the gas reservoir.

In view of this finding, and the identified shortcomings with the Dost *et al.* (2004) model for this application, an alternative GMPE was sought. The first consideration was that there is no existing equation applicable over the full range of magnitudes considered in the hazard integrations, that is, M_w 1.5–6.5. The choice was therefore made to adopt an empirical equation well calibrated at larger magnitudes, and then adjust the extrapolation to smaller magnitudes to fit the Groningen data. The GMPEs for PGA and PGV recently derived by Akkar *et al.* (2014) from European and Middle Eastern strong-

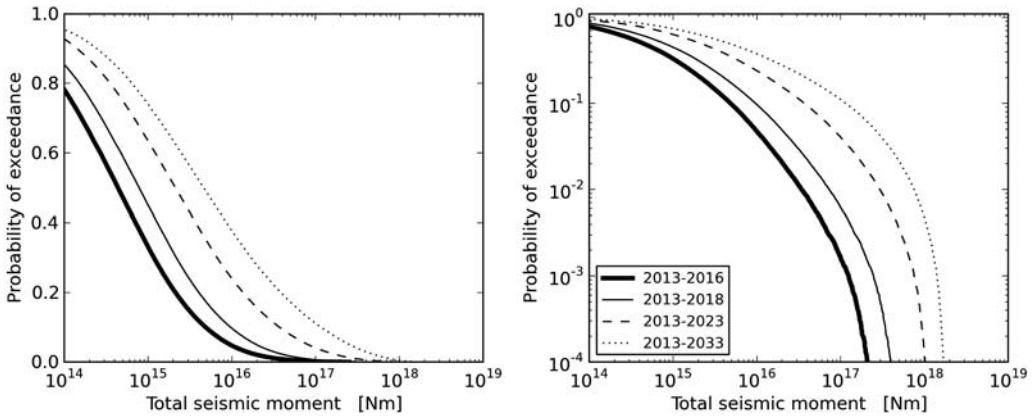

Figure 3. The probability distribution of total seismic moment for four different time intervals based on the seismological model of reservoir compaction in the Groningen field. The left panel shows these distributions on a log–linear scale and the the right panel shows the same distributions on a log–log scale.

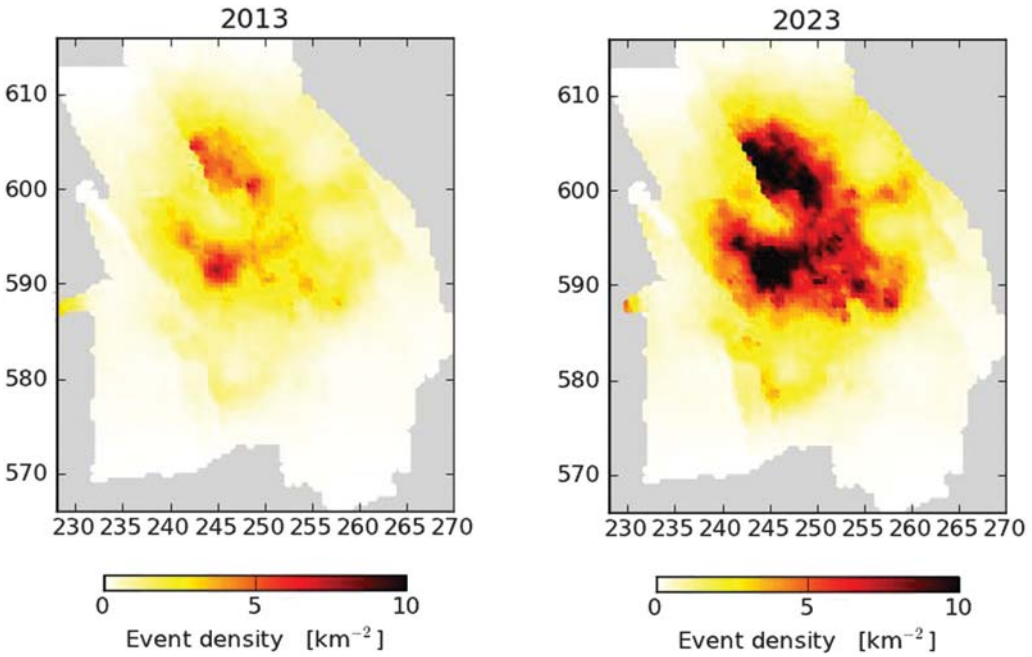

Figure 4. Event density maps for (left) 2013 and (right) 2023 based on the seismological model of reservoir compaction in the Groningen field.

motion data, were judged suitable in this regard, having been derived using data from earthquakes of M_w 4 and greater. These equations include V_{S30} as an explicit parameter and include the influence of soil nonlinearity, which made it suitable for the soft soil conditions that pervade across most of the Groningen field. The true benefits of this feature are of course limited because the equation models a generic European site response that might be quite different from the specific dynamic characteristics of the field. In subsequent revisions, the intention will be to develop a GMPE for rock conditions and combine these with local site amplification factors, but the currently available velocity data for the field is inadequate for this purpose. Another advantage of the Akkar *et al.* (2014) GMPE is that it provides versions with point-source as well as extended-source distance metrics. This feature allows the simplifying assumption (for computational efficiency) of modeling all earthquakes, including larger events, as point sources (hypocenters) without the need to generate virtual fault ruptures in the hazard simulations (Bommer and Akkar, 2012). The R_{hyp} model is chosen with a view to capturing the effect of the shallow focal depths of the Groningen earthquakes, although this may be somewhat conservative if, as noted previously, these shallower events are also associated with lower stress drops. A number of recent studies of motions from both natural (e.g., Allen, 2012) and induced (e.g., Hough, 2014) earthquakes conclude that shallow events tend to have lower stress drops. The GMPE also provides the between- and within-events of the aleatory variability.

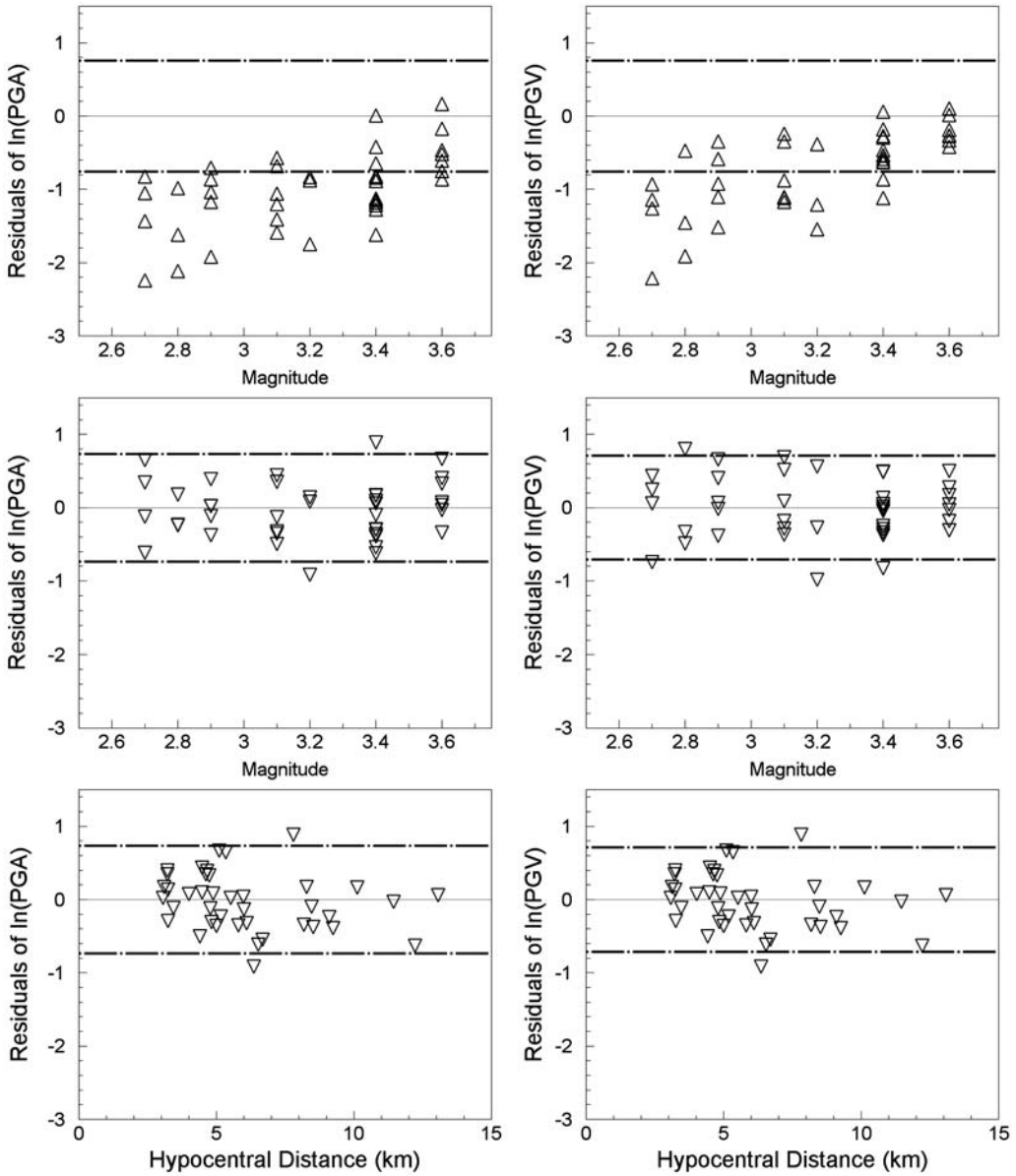

Figure 5. Residuals of peak ground acceleration (PGA; left) and peak ground velocity (PGV; right), calculated as the natural logarithm of the ratio of observed to predicted values, calculated using the Dost *et al.* (2004) equations (top row) plotted against magnitude. The broken lines indicate plus and minus one standard deviation. The middle and lower rows show the residuals with respect to the modified Akkar *et al.* (2014) ground-motion prediction equation (GMPE), against magnitude and distance, respectively. Although it is typically more appropriate to show between-event residuals against magnitude and within-event residuals against distance, the small database available here makes it difficult to separate these components, hence total residuals are shown.

The Akkar *et al.* (2014) GMPE overpredicts the field data slightly more severely than the Dost *et al.* (2004) equations, the residuals showing a similar trend with magnitude. The approach adopted was to maintain the original Akkar *et al.* (2014) equations for the magnitude range for which they were derived and then adjusting the model at lower magnitudes to match the recordings, in a similar fashion to the adjustments of the Chiou and Youngs (2008) equation to match small-magnitude recordings from California (Chiou *et al.*, 2010). For application to smaller magnitudes, the Akkar *et al.* (2014) functional form was adjusted by introducing additional magnitude-dependent terms in the magnitude-scaling term, the magnitude-dependent multiplier on the attenuation term, and the fictitious depth term, such that at around M_w 4 these adjustments would become equal to zero. Figure 5 shows the residuals of the data with respect to the adjusted equations for PGA and PGV, from which it can be seen that no strong trends are apparent. As discussed earlier, the Akkar *et al.* (2014) GMPEs, in common with most empirical equations, may be overestimating ground motions at this lower limit of their applicability, even if residual analyses in that study did not reveal such an effect. However, if this is

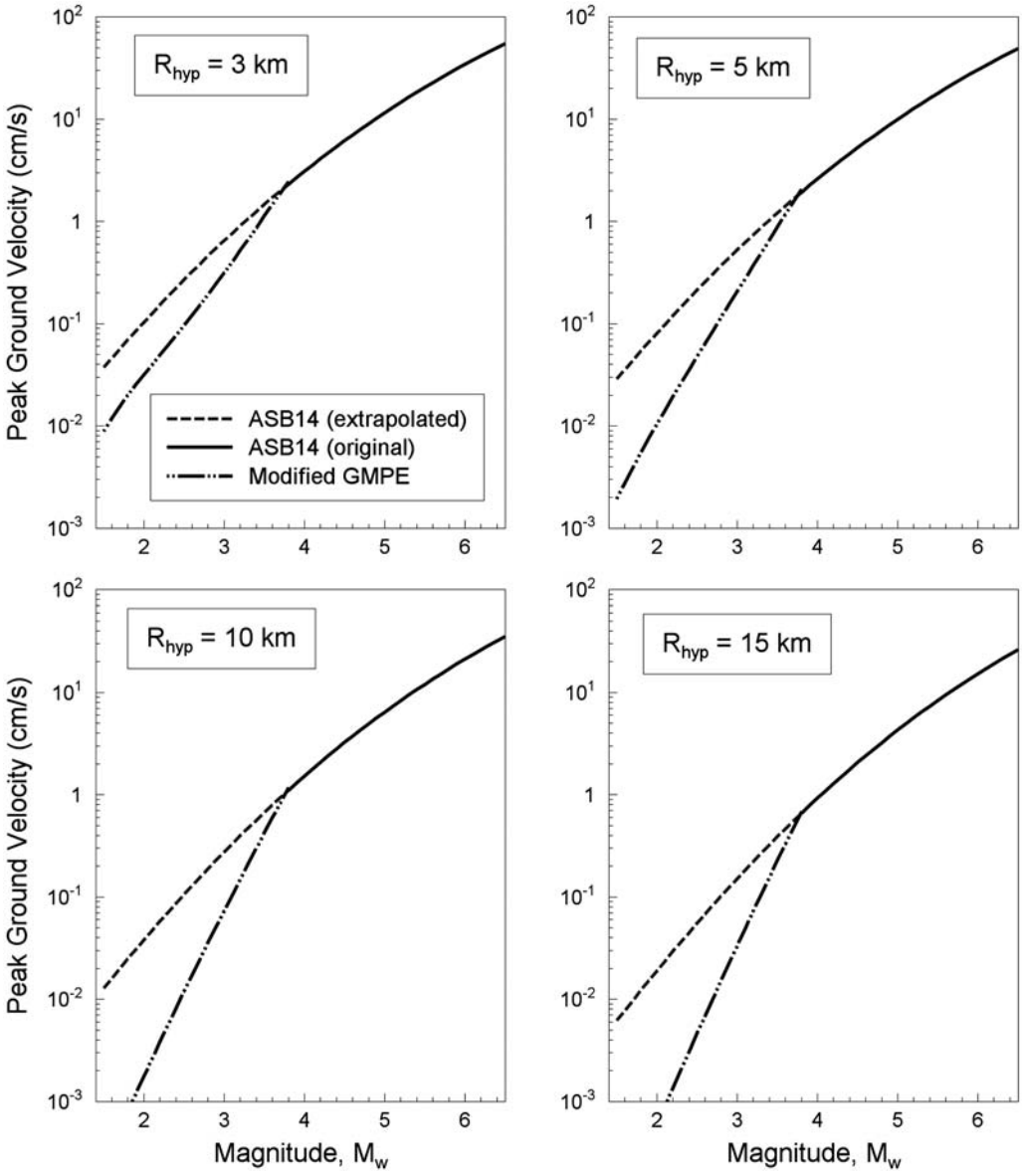

Figure 6. Magnitude scaling of PGV at different hypocentral distances (3, 5, 10, and 15 km) according to the GMPE of Akkar *et al.* (2014) and its adjustment to fit the Groningen data at small magnitudes.

the case then we consider the potential overestimation of motions for events of around M_w 4 to be acceptable for this preliminary model, which will be refined as more data become available.

The modified equation for PGV is illustrated in Figure 6, which shows the scaling with magnitude at different distances; the form of the PGA equation is similar. The plots are generated using the assumed parameters for application to the Groningen field, namely normal faulting and $V_{S30} = 200$ m/s. The PGV predictions are equal to those from the original equation for M_w 3.8 and greater, the PGA value from M_w 4.2 and above. The resulting equations have a rather sharp break in magnitude scaling, particularly at longer distances, as a result of the very different behavior at small and large magnitudes. This is, however, not inconsistent with the observations of Douglas and Jousset (2011) who noted that to cover the full variation of scaling behavior over a wide range of magnitudes would require a cubic function. Using the European GMPEs of Bindi *et al.* (2014), another viable candidate because it also includes an R_{hyp}-based model, would probably have resulted in a less abrupt adjustment because this equation has stronger magnitude scaling in the small-magnitude range. However, the Bindi *et al.* (2014) equations do not include nonlinear soil response. No clear case exists to select which equation is the most appropriate, especially because in the larger magnitude range multiple models will ultimately be required to capture epistemic uncertainty, whether through use of several equations or scaling a single backbone GMPE (Atkinson *et al.*, 2014). The important issue is that the resulting model is consistent with the local data at small mag-

nitudes and with ground motions from tectonic earthquakes at larger magnitudes, and satisfies the other requirements specified for the preliminary model.

The number of data points used for the adjustment to the model at lower magnitudes is too small to allow a reliable estimate of the standard deviation. Therefore, it was simply assumed that the sigma values of the Akkar *et al.* (2014) model hold across the entire magnitude range. Although many modern GMPEs model the standard deviation as varying with magnitude, with larger sigma values at small magnitude (e.g., Strasser *et al.*, 2009), it was not considered necessary to increase the value at lower magnitudes because the sigma of Akkar *et al.* (2014) is already large and calculated using data from earthquakes as small as M_w 4. We noted that the sigma values presented by Douglas *et al.* (2013) for their GMPEs for induced earthquakes are even larger, in particular the between-event component, but this may partly arise from uncertainties associated with the site classifications for the recording sites in their database, which come from several different regions. Given that the Groningen earthquakes are essentially occurring within a single source (the gas reservoir) and the waves are propagating to the surface through comparable paths to the epicenters, one could make a case for smaller sigma values. The residuals shown in Figure 5, although too small in number to be reliable in this regard, do not suggest that the sigma value should be increased. For this preliminary model, we consider the assumption of a constant sigma value across the full magnitude range to be appropriate and defensible.

A point that is important to acknowledge is that there is, of course, considerable epistemic uncertainty associated with both the median predictions and the sigma values for both small and large induced earthquakes. In the small magnitude range, the uncertainty arises from the small sample of data that has been used to constrain the model. The implicit assumption is that the ground motions produced by induced earthquakes in the M_w 4 to 6.5 range would be essentially the same as those from tectonic earthquakes of comparable size. This assumption is subject to very considerable epistemic uncertainty because there are no local data to substantiate this assumption hence the range of uncertainty for ground-motion predictions for these magnitudes will inevitably be even greater than that associated with predictions for natural seismicity. The quantification of epistemic uncertainty and its influence on the hazard estimates are discussed in a later section.

Hazard Simulation Results

The following ground-motion hazard results were obtained using the linear compaction model, the current production plan, and the modified Akkar *et al.* (2014) GMPE for the 10 years from 2013 to 2023.

Figure 7 shows a series of diagnostic plots to verify that the simulated distributions match the parent distributions for the total seismic moment, the frequency–magnitude, and the maximum magnitude distributions. The simulated total seismic moment closely follows the parent distribution as expected (Fig. 7a). The largest deviations occur for the largest moments approaching 10^{18} N·m. These have an occurrence rate of 1 in every 1000 catalogs simulated so the finite sample obtained after simulating 10^5 catalogs is just about 100 events. The 95% Poisson confidence interval associated with counting such a small number of events is, however, still consistent with the parent distribution.

The frequency–magnitude distribution of all simulated events (Fig. 7c) reproduces the slope corresponding to $b = 1$ from the parent distribution for the first event and is also consistent with the maximum magnitude of a single event never exceeding M_{max} 6.5. The simulated distribution differs from the initial parent distribution simply because the parent distribution changes with each simulated event as M_{max} is reduced from its initial value of M_w 6.5 to ensure the next simulated event does not cause the total seismic moment of simulated events to exceed the target for that catalog. This yields a composite parent distribution that truncates over a wider range of magnitudes than the initial parent distribution indicated in the figure.

Ground-motion results obtained for each surface observation point form continuous hazard curves representing the expected rate of exceedance with respect to PGV and PGA (Fig. 8). These curves all exhibit a similar monotonic decline in the expected exceedance rate with increasing ground motion.

Figure 9 shows PGV and PGA with an exceedance probability of 2% over 10 years, equivalent to 10% over 50 years or a 475-year return period, as used in many seismic design codes, including Eurocode 8 (2004). This is adopted as a convenient reference, despite the somewhat arbitrary origins of this widely used probability level (Bommer and Pinho, 2006), not because it is considered the most appropriate way to represent hazard in this application. The areal distribution of ground-motion hazard conforms to the distribution of expected event densities (Fig. 4) that are in turn predicted to conform to the distribution of reservoir compaction.

Disaggregation of the Seismic Hazard

The ground-motion hazard maps shown in the previous section were obtained by aggregating all exceedances of the chosen ground-motion thresholds and averaging the exceedance rates over all the simulated catalogs. This process of aggregation keeps track of the combinations of event magnitude, distance, and GMPE variability giving rise to the ground-motion exceedance rates.

Disaggregation is the process of looking at the hazard in terms of the magnitude, hypocentral distance, and GMPE variability of the events giving rise to it (McGuire, 1995; Bazzurro and Cornell, 1999), so that questions such as "What event magnitudes and hypocentral distances contribute most to the hazard?" can be answered in a useful way. Disaggregation of the Monte Carlo simulation results is straightforward as information about the magnitude, distance, and the stochastic part of the GMPE (epsilon) may simply be retained for each instance of ground motion at each surface observation point.

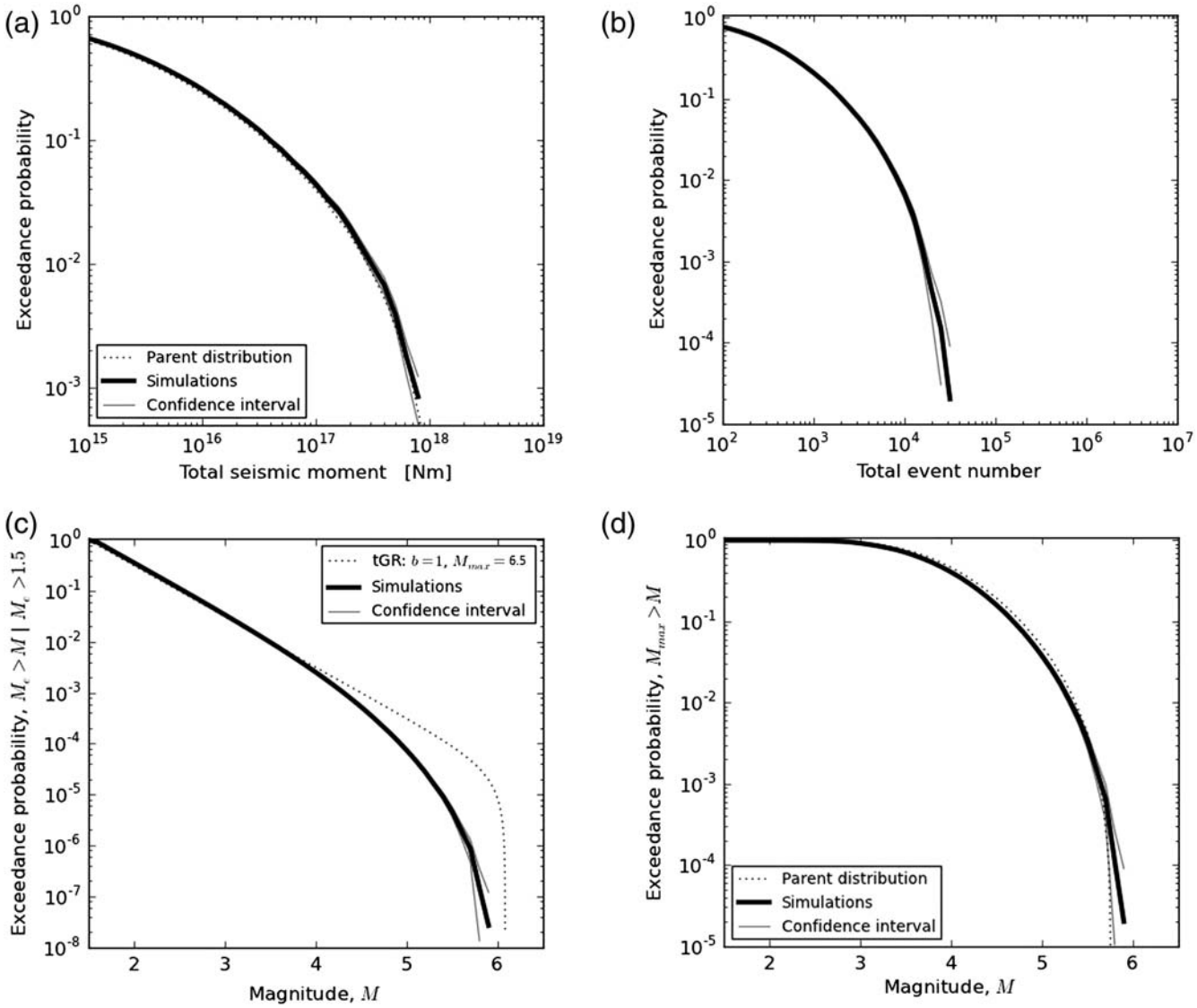

Figure 7. Diagnostic plots for the distribution of (a) total seismic moment, (b) total event count, (c) magnitude, and (d) maximum magnitude for the Monte Carlo results obtained after simulating 10^5 catalogs representing $M_w \geq 1.5$ earthquakes induced by gas production over the interval 2013–2023 based on the current production plan, and the current reservoir compaction and seismic-strain partitioning models. tGR, truncated Gutenberg-Richter frequency-magnitude distribution.

These may then be presented as frequency distributions for individual observation points (e.g., Bazzurro and Cornell, 1999) (Figs. 10 and 11) or as the map distribution of some characteristic metric of these distributions, such as the average or modal value (e.g., Harmsen *et al.*, 1999).

Figure 10a shows the occurrence rate of PGV versus magnitude, distance, and the GMPE epsilon within small bins. Gray denotes the absence of any counts in any of the 10^5 simulated catalogs over the 10-year period 2013–2023. For any particular PGV threshold, the total exceedance rate corresponds to the sum of rates over all the bins located above the threshold. Similarly, the partial exceedance rate due to a particular magnitude bin is the sum of rates in all bins corresponding to that magnitude above the PGV threshold; and also for distance and epsilon. Likewise, Figure 11a shows the same disaggregation for PGA. The relative contribution to the ground-motion hazard is then measured as the ratio of the partial to the total exceedance rates (Figs. 10b and 11b).

It is particularly instructive to understand which magnitudes contribute most to the hazard. Referring to the magnitude plots, notice that the hazard is dominated by the intermediate magnitudes. The largest contribution to the hazard with a mean recurrence rate equivalent to 2% over 10 years is M_w 5.0 for PGV and M_w 4.2 for PGA. Events with magnitudes approaching the maximum magnitude of M_w 6.5, say $5.5 \leq M_w < 6.5$ are so rare that they exert almost no influence on the hazard for these recurrence rates. Of much greater significance for the hazard are the less rare events of intermediate magnitude, $4 \leq M_w \leq 5$, typically occurring at smaller hypocentral distances. An important conclusion that

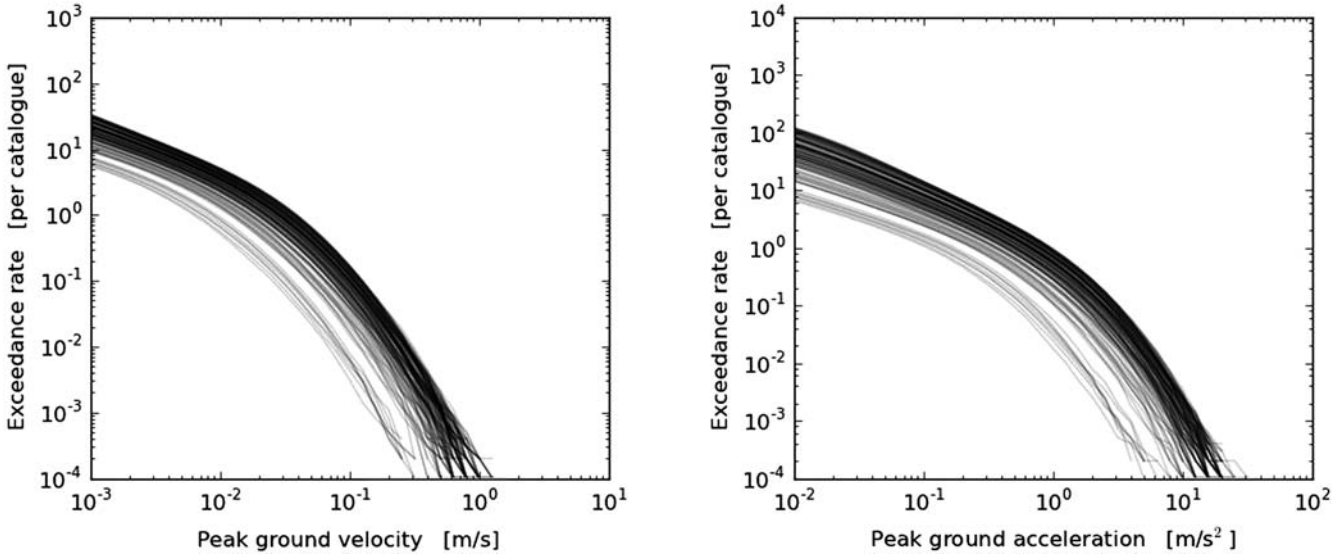

Figure 8. Ground-motion hazard curves obtained by Monte Carlo simulation of 10^5 catalogs representing $M_w > 1.5$ earthquakes induced by gas production over the interval 2013–2023 based on the current production plan, and the current reservoir compaction and seismic-strain partitioning models.

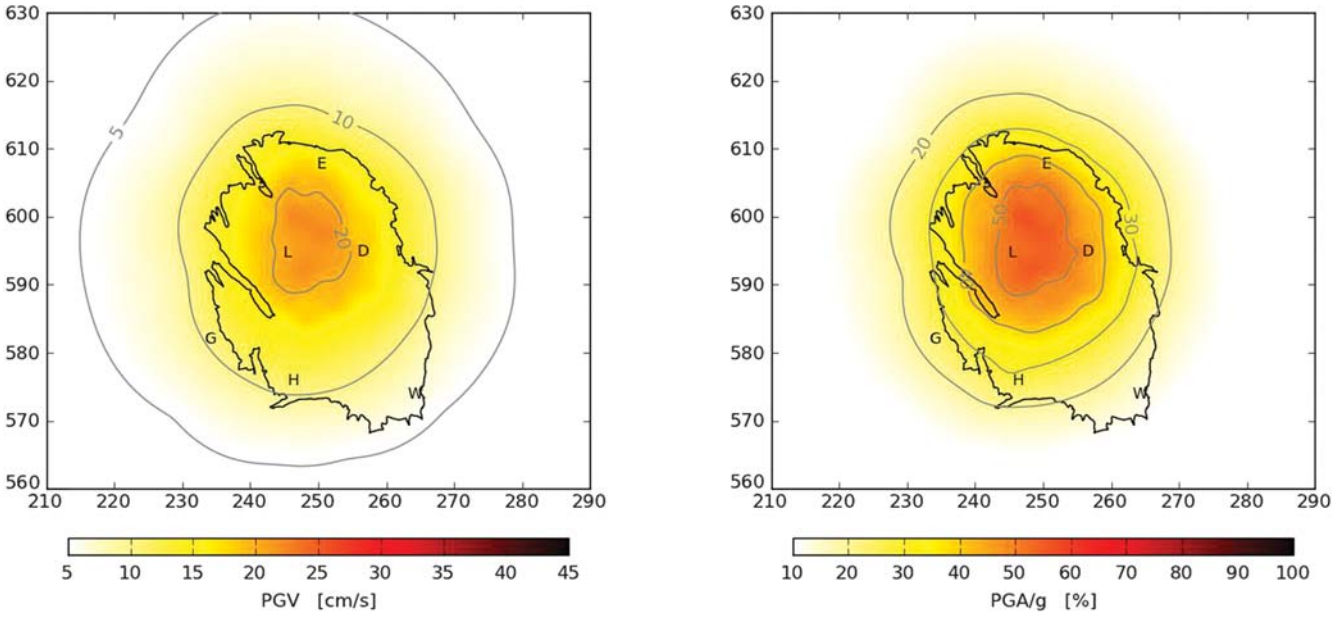

Figure 9. Predicted ground motion with a 2% chance of exceedance for the 10 years from 2013 to 2023. Maximum ground motions are a PGV of 22 cm/s and a PGA of 0.57g, located above the region of greatest reservoir compaction. The black line denotes the outline of the field and the letters D, E, G, H, L, and W denote the place names Delfzijl, Eemshaven, Groningen, Hoogezand, Loppersum, and Winschoten, respectively.

is drawn from this observation is that the influence of the maximum magnitude is secondary and it is not useful to focus exclusively on this parameter as the primary characterization of the hazard, given that it corresponds to an extremely unlikely event which barely contributes to the hazard at the probabilities of interest.

Figure 11 shows that the PGA levels for a 2% probability of exceedance are driven by earthquakes of moderate magnitude; the modal contributions are from M_w 4.2 earthquakes. This value is close to or even below the minimum magnitude thresholds generally considered in conventional PSHA, which should be borne in mind if the hazard results are compared with those obtained for natural seismicity in other regions. Consequently, the seismic hazard associated with $M_w \geq 5$ events is substantially smaller (e.g., Fig. 12).

The exact magnitude threshold for damage to occur will clearly depend on several factors, including earthquake depth and building vulnerability. We do not apply a minimum mag-

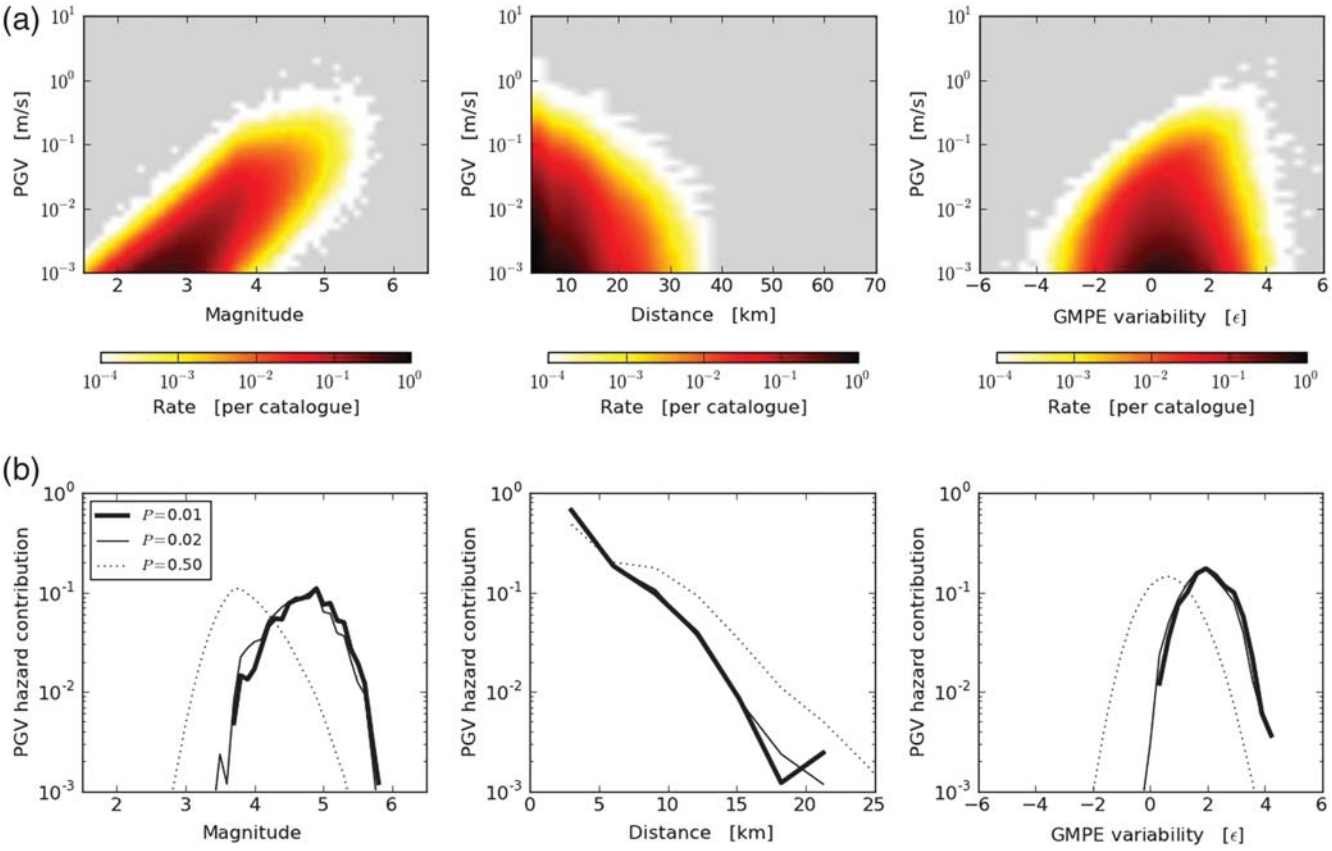

Figure 10. (a) Occurrence rates for PGV as a function of magnitude, distance, and GMPE epsilon, ϵ, for a single surface location directly above the region of maximum reservoir compaction. Gray denotes no occurrence in any of the simulations. (b) The fractional contribution to the ground motion with a probability of exceedance of $p = 0.01$, 0.02, 0.5 from 2013 to 2023.

nitude cutoff that affects the PSHA results for the Groningen field to provide an unfiltered quantification of the hazard. However, the influence of the earthquake magnitude on the damage potential will need to be taken into account in the risk calculations that follow. If fragility functions adopted for the buildings in the area are calibrated to typical damaging earthquakes, for $M \geq 6$, then using the PGA and PGV values obtained from the PSHA dominated by smaller magnitudes will lead to overestimation of damage and losses.

Another important observation about these disaggregation results is that the dominant contribution to the hazard from the stochastic part of the GMPE comes from $\epsilon = 2$, about two standard deviations above the median value of $\epsilon = 0$. This reflects the large number of simulated earthquakes in the intermediate magnitude range that allows epsilons as large as 2 to be sampled frequently enough to drive the hazard.

Epistemic Uncertainty and Hazard Sensitivity

True statistical variability, known as aleatory variability, represents the stochastic nature of a process and is addressed in the approach described here by random sampling of the appropriate distributions in the Monte Carlo simulation process. Epistemic uncertainty characterizes uncertainty either in the values of parameters which are fixed but are known only to within a certain accuracy, or with the choice of particular models. Significant epistemic uncertainties exist in the seismic-hazard assessment for the Groningen field; these are primarily associated with strain partitioning, the choice of GMPE, and reservoir compaction. Variation of the *b*-value with compaction may also be a potentially significant source of epistemic uncertainty. As part of the ongoing work to quantify the seismic hazard (and the associated risk) due to induced earthquakes in the Groningen field, in addition to refining each of the elements of the model presented herein, we shall undertake the work of identifying and quantifying all sources of epistemic uncertainty and assess their impact on the final estimates. For the purpose of representing and incorporating the epistemic uncertainties into the hazard assessment, we are likely to use a logic-tree structure, in which each branch of the logic-tree represents a distinct scenario of a particular model and associated parameter values, and is assigned a weight representing the relative merit or degree of belief in each of the alternatives. These weights are treated as (subjective) probabilities in subsequent calculations. The Monte Carlo simulation approach adopted for this hazard study can then easily be extended to sample from the discrete probability distributions represented by the logic-tree branches.

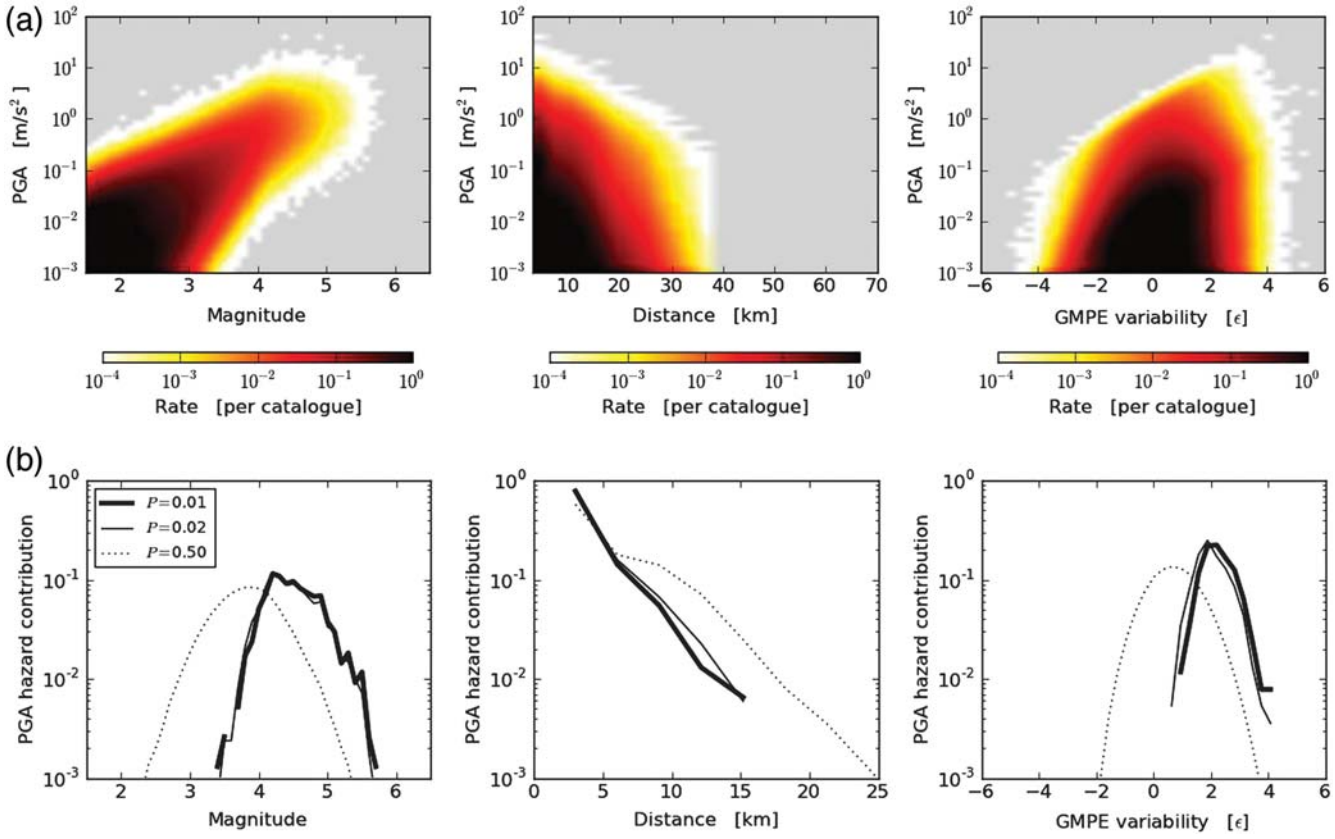

Figure 11. Same as Figure 10, except for PGA.

Several sources of epistemic uncertainty are associated with the seismological model underlying the hazard assessment calculations, including future production levels. For a given production scenario, the resulting compaction, which drives the generation of earthquakes in the strain-partitioning model, is subject to considerable uncertainty. Future compaction may be predicted using a range of possible models, constrained by geodetic measurements of surface displacements and reservoir compaction. These measurements are, however, not sufficient to unambiguously indicate which of several possible compaction models should be used. For the analysis presented in the main body of the article, a linear poroelastic compaction model (Bourne *et al.*, 2014) was used, but at least two alternative higher-order models, time-decay and isotach, could be used in its place and might therefore occupy alternative branches on the logic tree. Reservoir compaction within the time-decay model depends on the state and time history of pressure depletion (Mossop, 2012). Reservoir compaction within the isotach model depends on the state and rate of pressure depletion (de Waal, 1986). Both alternative models provide similar matches to the observed history of surface subsidence, but compute slightly different results for future reservoir compaction.

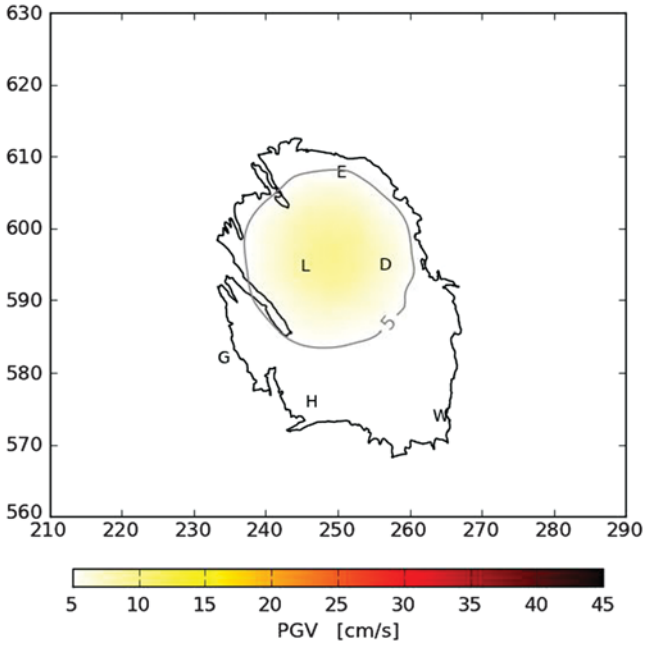

Figure 12. Predicted PGV with a 2% chance of exceedance, for the 10 years from 2013 to 2023 for $M \geq 5.0$.

The Gutenburg–Richter *b*-value characterizing the Groningen earthquake catalog might be expected to have a strong influence on the calculated hazard because the *b*-value, being the slope of the frequency–magnitude distribution, expresses the relative abundances of small and large events in an earthquake catalog. Bourne *et al.* (2014) show evidence for variation of the *b*-value with compaction when

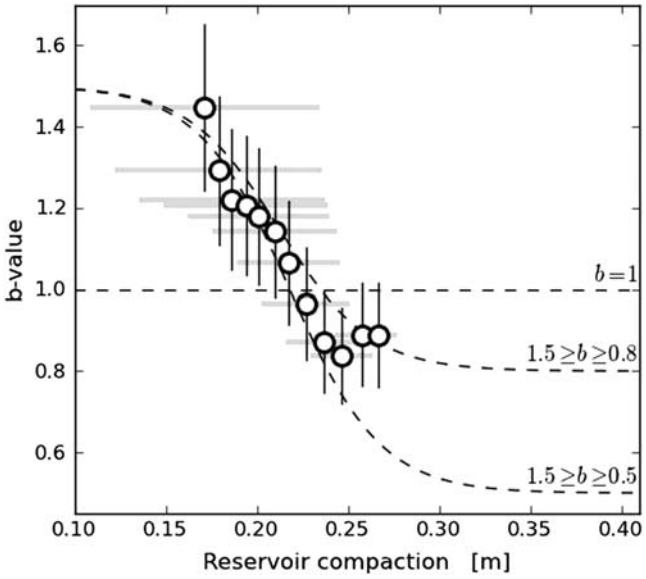

Figure 13. Three different models for the variation in b-value with reservoir compaction. Two of these models are parametrized as hyperbolic tangent functions to represent two possible fits to the observed b-values. The other model represents the possibility that $b = 1$ and this apparent variation with compaction is a bias due to the small samples of earthquakes within each compaction interval.

the Groningen catalog is divided into subcatalogs defined by compaction bins (Fig. 13). In the hazard analyses presented in this article, a constant value of $b = 1$ was used, but alternative scenarios could be defined by two compaction-dependent hyperbolic tangent functions, with $0.5 \le b \le 1.5$ and $0.8 \le b \le 1.5$, respectively. The $0.8 \le b \le 1.5$ scenario fits the upper envelope of the data. The $0.5 \le b \le 1.5$ scenario fits the lower envelope of the data and has been extended to cover what is usually accepted to be the full range of physically permissible b-values when a finite moment budget is assumed. This sensitivity was explored and the b-value variations considered found to have negligible impact on the calculated hazard; it seems that the competing influences of increasing event size, but reduced event number (for the large events) corresponding to reductions in the b-value, approximately balance each other out, at least in this case.

There is also very significant uncertainty in the future evolution of the value of the strain-partitioning factor which determines the proportion of strain expressed as earthquakes. The current values depend on compaction, but are typically in the range 10^{-4} to 10^{-3} and any future unmodeled increase would have a material effect on the hazard. However, the relative contributions of epistemic and aleatory components of uncertainty are unknown and this would need to be addressed to develop the complete logic tree. At the same time, it is conceivable that an alternative model, for example, based on the activity rates rather than on the strain partitioning, could be developed and included in the logic tree as an alternative seismological source model.

Another very clear source of epistemic uncertainty is associated with the ground-motion prediction model. The key uncertainty is that related to the median predictions for larger magnitude earthquakes, for which there is currently no data to constrain the model. However, there is potential for improvement in this respect, through the use of full waveform modeling of earthquakes originating in the gas reservoir and also detailed dynamic characterization of the near-surface layers in the field, both of which are now underway. The strong-motion recording networks in the field are also being expanded, such that many more records will become available from future earthquakes. Although this may not reduce the uncertainty associated with predicting motions from moderate-to-large magnitude earthquakes, it will provide much stronger constraint on the sigma value in the model, and possibly also allow the estimation of nonergodic sigmas once multiple recordings are available from some of the recording stations.

Although outside the scope of this article, the uncertainties in the hazard model will ultimately need to be combined with those associated with the characterization of the exposed building stock and its fragility (e.g., Crowley *et al.*, 2005).

Discussion and Conclusions

We have developed a method for PSHA suited to the time-dependent induced seismicity associated with conventional gas production. We make use of the moment–strain relationship of Kostrov (1974) and McGarr (1976) to relate total seismic moment released to bulk volume change of a compacting reservoir. Monte Carlo methods are used to calculate the rates of exceedance of specified thresholds of ground motion (PGV and PGA) from a geomechanical model of reservoir compaction according to a given gas production plan. Our approach is illustrated by application to the case of the induced seismicity associated with gas production from the Groningen field located in the northeast of The Netherlands where the hazard due to natural seismicity is extremely low (Giardini *et al.*, 2013).

Because of the time dependence of induced seismicity, in addition to choosing the hazard metric it is also necessary to choose a time interval for the hazard assessment. Maximum values of predicted ground motion with a 2% chance of exceedance (if the hazard were time invariant, this would be equivalent to the 475-year return period taken as a standard in Eurocode 8) for the period from 2013 to 2023, are a PGV of 22 cm/s and a PGA of $0.57g$. These maximum values are found above the area of greatest reservoir compaction.

Disaggregation, the process of looking at the hazard in terms of the magnitude, hypocentral distance, and GMPE variation of the events giving rise to it shows that earthquakes of intermediate magnitudes, M_w 4–5, at hypocentral distances of 3 km, make the largest contributions to the calculated hazard. Events with larger magnitudes, approaching the maximum possible-induced earthquake of M_w 6.5 that corresponds to the exceptional case of all induced strain being released in a single event at the end of production, are so extremely rare in the modeled catalogs that they exert almost no influence on the hazard for the return rates considered.

In interpreting the seismic-hazard results presented, it is important to appreciate a key difference with most previous works on seismic hazard and risk which generally concern themselves with the occurrence of large damaging natural earthquakes (e.g., $M_w > 5$). Care must be taken in making any comparisons of the results of this study with 475-year return period hazard maps for natural seismicity developed for engineering design purposes, such as the current national hazard maps for the United States (Petersen *et al.*, 2014) and the new SHARE map for Europe (Giardini *et al.*, 2013); the former used a lower magnitude limit of M_w 5, the latter a minimum threshold of M_w 4.5. The disaggregation of the Groningen field seismic-hazard analysis shows that the largest contributions are due to small-to-intermediate magnitudes (M_w 4–5). Therefore, the application of a lower magnitude limit such as those used in normal seismic-hazard mapping would lead to drastic reductions of the resulting ground-motion amplitudes.

The magnitude range covered by the hazard calculations, and the consequent magnitude range driving the hazard, must be taken into account in the risk analysis for which these hazard calculations will ultimately form the basis. Structures for which the stiffness and strength degrade appreciably under successive cycles of loading, such as the unreinforced masonry that dominates much of the building stock in Europe, are sensitive to the duration of the ground shaking (e.g., Bommer *et al.*, 2004). The fragility curves used for estimating damage and losses, especially for the more severe damage states that can pose a threat to life and limb, must be appropriately calibrated to the short durations of motion expected from such small earthquakes (Bommer *et al.*, 2015). This is particularly true given that the disaggregation results indicate that the modal contribution to PGA and PGV levels are due to small-to-intermediate magnitude (M_w 4–5), the shortest hypocentral distances (3 km), and epsilon values that are two standard deviations above the median prediction ($\epsilon = 2$). For a given PGV or PGA value, lower magnitudes imply a shorter duration due to the scaling of duration with magnitude, and likewise shorter hypocentral distances, although to a lesser extent. Higher epsilon values also would imply even shorter than average durations given the negative correlation between these parameters and the duration of shaking (Bradley, 2011).

The hazard model presented herein is considered preliminary, its primary purpose being to develop a complete methodological approach, with all elements calibrated to currently available field data, for estimating the ground-shaking hazard in terms of PGA and PGV. The work is ongoing and each component of the model is being refined, through extensive data collection, and the associated epistemic uncertainty will be quantified in parallel. As previously indicated, there are several important sources of epistemic uncertainty, and Nederlandse Aardolie Maatschappij B.V. (NAM) is investing in extensive data gathering to reduce these as far as possible. For example, laboratory compaction experiments as well as further acquisition and analysis of the geodetic surface deformation data are planned to address the uncertainty in the reservoir compaction model that exists due to nonuniqueness in the fit to observed surface subsidence. The ambiguity in the fit leaves open the possibility of a delay between pore-pressure depletion and reservoir compaction or a dependence on both the rate and state of pore-pressure depletion.

The model of strain partitioning as a function of reservoir compaction is subject to considerable uncertainty due to the limited number of observed earthquakes. This allows the possibility of important, yet-to-be identified, mechanisms that influence the strain partitioning. For instance, strain partitioning may depend on compaction rate as well as compaction, or there may be a time delay between changes in compaction and changes in seismicity, or there may be a spatial variability in strain partitioning due to preexisting faults or some other geological heterogeneity such as clay content. To address this uncertainty, an enhanced seismic monitoring network for the Groningen field will be deployed in 2014–2015 to provide a total of ~70 boreholes of 200 m depth instrumented with geophone arrays (in addition to five such boreholes already operated within and around the field by KNMI), with a projected magnitude of detection completeness of M_w 0.5. In addition to refining the strain-partitioning model, work is also underway to develop an alternative approach in which the earthquake activity rate (rather than total moment release) is related to the reservoir compaction.

The GMPEs will be extended to predict not only PGA and PGV, but also spectral accelerations at multiple response periods (corresponding to the vibration periods of the exposed building stock) and probably also ground-motion durations conditioned on accelerations. As well as the expanded KNMI accelerograph network (18 instruments) now operating in the field, surface accelerographs are being installed collocated with the ~70 geophone boreholes mentioned above. Extensive *in situ* measurements (including boreholes, seismic cone penetration test, and multi-channel analysis of surface waves) will be conducted at these locations to provide detailed shear-wave velocity profiles, providing a much richer local database. The intention is to derive new GMPEs, with continuous functional forms, constrained by this local data at the small-magnitude range and by recordings from tectonic earthquakes at larger magnitudes. Additional constraint on the functional form and the range of alternative extrapolations to larger magnitudes will be provided by both full waveform modeling and stochastic simulations using the output from inversions of the local surface and borehole data.

Future publications will present the progress made on all the activities outlined in the preceding paragraphs. Our hope is that this article will serve as a useful contribution to the developing body of knowledge and experience to quantify the hazard from induced seismicity.

Data and Resources

Monte Carlo simulations were implemented using SciPy. Most of the figures were created using Matplotlib (Hunter, 2007). The earthquake catalog was provided by Koninklijk Nederlands Meteorologisch Instituut (KNMI).

These data may be obtained from KNMI at www.knmi.nl (last accessed December 2013). The geodetic subsidence data and reservoir compaction model were provided by Nederlandse Aardolie Maatschappij B.V. and are proprietary.

Acknowledgments

We gratefully acknowledge our colleagues Jan Willem Jacobs, Rob van Eijs, Onno van der Waal, and Anthony Mossop from Nederlandse Aardolie Maatschappij, and Ibbel Ansink and Dirk Smit from Shell Global Solutions International, for their significant support during this study. Many stimulating discussions with Dirk Kraaijpoel (Koninklijk Nederlands Meteorologisch Instituut), Karin van Thienen-Visser and Jaap Breunese (TNO), Annemarie Muntendam-Bos and Hans de Waal (Staatstoezicht op de Mijnen) also helped to improve this work. Rui Pinho and Helen Crowley generously shared their knowledge of building vulnerability and seismic risk. Ian Main is thanked for a careful review of an early draft of this article. We also thank Ivan Wong, John Douglas, and another reviewer for their useful suggestions that helped us to make improvements to the text. Finally the authors wish to thank Nederlandse Aardolie Maatschappij and Shell Global Solutions International for granting permission to publish this article.

References

Akinci, A., F. Galadini, D. Pantosi, M. Petersen, L. Malagnini, and D. Perkins (2009). Effect of time dependence of probabilistic seismic-hazard maps and deaggregation for the Central Apennines, Italy, *Bull. Seismol. Soc. Am.* **99,** no. 2A, 585–610.

Akkar, S., M. Sandkkaya, and J. J. Bommer (2014). Empirical ground-motion models for point- and extended-source crustal earthquake scenarios in Europe and the Middle East, *Bull. Earthq. Eng.* **12,** no. 1, 359–387, Erratum: 12, no. 1, 389–390.

Al Atik, L., N. A. Abrahamson, J. J. Bommer, F. Scherbaum, F. Cotton, and N. Kuehn (2010). The variability of ground-motion prediction models and its components, *Seismol. Res. Lett.* **81,** no. 5, 783–793.

Allen, T. (2012). Stochastic ground motion prediction equations for south-eastern Australian earthquakes using updated source and attenuation parameters, *Technical Report*, Geoscience Australia, Canberra, Australia.

Assatourians, K., and G. M. Atkinson (2013). EqHaz: An open-source probabilistic seismic-hazard code based on the Monte Carlo simulation approach, *Seismol. Res. Lett.* **84,** no. 3, 516–524, doi: 10.1785/0220120102.

Atkinson, G. M., and M. Morrison (2009). Observations on regional variability in ground-motion amplitude for small-to-moderate magnitude earthquakes in North America, *Bull. Seismol. Soc. Am.* **99,** no. 4, 2393–2409.

Atkinson, G. M., J. Bommer, and N. Abrahamson (2014). Alternative approaches to modeling epistemic uncertainty in ground motion in probabilistic seismic-hazard analysis, *Seismol. Res. Lett.* **85,** no. 6, 1141–1144.

Bazzurro, P., and C. A. Cornell (1999). Disaggregation of seismic hazard, *Bull. Seismol. Soc. Am.* **89,** no. 2, 501–520.

Bindi, D., M. Massa, L. Luzi, G. Ameri, E. Pacor, R. Puglia, and P. Augliera (2014). Pan-European ground-motion prediction equations for the average horizontal component of PGA, PGV, and 5%-damped PSA at spectral periods up to 3.0 s using the RESORCE dataset, *Bull. Earthq. Eng.* **12,** no. 1, 391–430.

Bommer, J. J., and S. Akkar (2012). Consistent source-to-site distance metrics in ground-motion prediction equations and seismic source models for PSHA, *Earthq. Spectra* **28,** no. 1, 1–15.

Bommer, J. J., and J. E. Alarcón (2006). The prediction and use of peak ground velocity, *J. Earthq. Eng.* **10,** no. 1, 1–31.

Bommer, J. J., and R. Pinho (2006). Adapting earthquake actions in Eurocode 8 for performance-based seismic design, *Earthq. Eng. Struct. Dynam.* **35,** no. 1, 39–55.

Bommer, J. J., H. Crowley, and R. Pinho (2015). A risk-mitigation approach to the management of induced seismicity, *J. Seismol.* **19,** no. 2, 623–646, doi: 10.1007/s10950-015-9478-z.

Bommer, J. J., J. Douglas, F. Scherbaum, F. Cotton, H. Bungum, and D. Fäh (2010). On the selection of ground-motion prediction equations for seismic hazard analysis, *Seismol. Res. Lett.* **81,** no. 5, 783–793.

Bommer, J. J., G. Magenes, J. Hancock, and P. Penazzo (2004). The influence of strong-motion duration on the seismic response of masonry structures, *Bull. Earthq. Eng.* **2,** no. 1, 1–26, doi: 10.1023/B:BEEE.0000038948.95616.bf.

Bommer, J. J., P. Stafford, J. Alarcón, and S. Akkar (2007). The influence of magnitude range on empirical ground-motion prediction, *Bull. Seismol. Soc. Am.* **97,** no. 6, 2152–2170.

Bothara, J. K., R. P. Dhakal, and J. B. Mander (2010). Seismic performance of an unreinforced masonary building: An experimental investigation, *Earthq. Eng. Struct. Dynam.* **39,** no. 1, 45–68.

Bourne, S. J., S. J. Oates, J. van Elk, and D. Doornhof (2014). A seismological model for earthquakes induced by fluid extraction from a subsurface reservoir, *J. Geophys. Res.* **119,** 8991–9015, doi: 10.1002/2014JB011663.

Bradley, B. A. (2011). Correlation of significant duration with amplitude and cumulative intensity measures and its use in ground motion selection, *J. Earthq. Eng.* **15,** no. 6, 809–832.

Chiou, B., and R. Youngs (2008). An NGA model for the average horizontal component of peak ground motion and response spectra, *Earthq. Spectra* **24,** no. 1, 173–215.

Chiou, B., R. Youngs, N. Abrahamson, and K. Addo (2010). Ground-motion attenuation model for small-to-moderate shallow crustal earthquakes in California and its implications on regionalization of ground-motion prediction models, *Earthq. Spectra* **26,** no. 4, 907–926.

Convertito, V., N. Maercklin, N. Sharma, and A. Zoldo (2012). From induced seismicity to direct time-dependent seismic hazard, *Bull. Seismol. Soc. Am.* **102,** no. 6, 2563–2573.

Cornell, C. (1968). Engineering seismic risk analysis, *Bull. Seismol. Soc. Am.* **58,** 1503–1606.

Crowley, H., and J. J. Bommer (2006). Modelling seismic hazard in earthquake loss models with spatially distributed exposure, *Bull. Earthq. Eng.* **4,** no. 3, 249–273, doi: 10.1007/s10518-006-9009-y.

Crowley, H., J. Bommer, R. Pinho, and J. Bird (2005). The impact of epistemic uncertainty on an earthquake loss model, *Earthq. Eng. Struct. Dynam.* **34,** no. 14, 1635–1685.

Davies, R., G. Foulger, A. Binley, and P. Styles (2013). Induced seismicity and hydraulic fracturing for the recovery of hydrocarbons, *Marine Petrol. Geol.* **45,** 171–185.

de Crook, T., B. Dost, and H. W. Haak (1995). Analyse van het seismische risico in Noord-Nederland, *Technical Report*, Koninklijk Nederlands Meteorologisch.

de Crook, T., H. W. Haak, B. Dost, and d. T. Crook (1998). Seismisch risico in Noord-Nederland, *Technical Report*, Koninklijk Nederlands Meteorologisch.

de Waal, J. A. (1986). On the rate type compaction behaviour of sandstone reservoir rock, *Ph.D. Thesis*, Delft Technical University, Delft, The Netherlands.

Dost, B., and H. W. Haak (2007). Natural and induced seismicity, in *Geology of the Netherlands*, Th. E. Wong, D. Batjes, and J. de Jager (Editors), Royal Netherlands Academy of Arts and Sciences, Amsterdam, The Netherlands, 223–239.

Dost, B., and D. Kraaijpoel (2013). The August 16, 2012 earthquake near Huizinge (Groningen), *Technical Report January*, KNMI, de Bilt, The Netherlands.

Dost, B., M. Caccavale, T. V. Eck, and D. Kraaijpoel (2013). Report on the expected PGV and PGA values for induced earthquakes in the Groningen area, *Technical Report December*, KNMI, de Bilt, The Netherlands.

Dost, B., F. Goutbeek, T. V. Eck, and D. Kraaijpoel (2012). Monitoring induced seismicity in the North of the Netherlands: status report 2010, *Technical Report*, Koninklijk Nederlands Meteorologisch.

Dost, B., T. van Eck, and H. Haak (2004). Scaling of peak ground acceleration and peak ground velocity recorded in the Netherlands, *Boll. Geof. Teor. Appl.* **45,** no. 3, 153–168.

Douglas, J., and P. Jousset (2011). Modeling the differences in ground-motion magnitude-scaling in small and large earthquakes, *Seismol. Res. Lett.* **82,** no. 4, 504–508.

Douglas, J., B. Edwards, V. Convertito, N. Sharma, A. Tramelli, D. Kraaijpoel, B. M. Cabrera, N. Maercklin, and C. Troise (2013). Predicting ground motions from induced earthquakes in geothermal areas, *Bull. Seismol. Soc. Am.* **103,** no. 3, 1875–1897.

Ebel, J. E., and A. L. Kafka (1999). A Monte Carlo approach to seismic hazard analysis, *Bull. Seismol. Soc. Am.* **89,** 854–866.

Eck, v. T., F. Goutbeek, H. Haak, and B. Dost (2006). Seismic hazard due to small-magnitude, shallow-source, induced earthquakes in The Netherlands, *Eng. Geol.* **87,** nos. 1/2, 105–121, doi: 10.1016/j.enggeo.2006.06.005.

Ellsworth, W. (2013). Injection-induced earthquakes, *Science*, **341,** no. 6142, 250–260, doi: 10.1126/science.1225942.

Eurocode 8 (2004). Design of structures for earthquake resistance, part 1: General rules, seismic actions and rules for buildings, *Technical Report*, Comité Européen de Normalisation (CEN), Brussels.

Evans, K., A. Zappone, T. Kraft, N. Deichmann, and F. Moia (2012). A survey of the induced seismic responses to fluid injection in geothermal and CO_2 reservoirs in Europe, *Geothermics* **41,** 30–54.

Giardini, D., J. Woessner, L. Danciu, H. Crowley, F. Cotton, G. Grünthal, R. Pinho, and L. Valensise (2013). *Seismic Hazard Harmonization in Europe (SHARE): Online Data Resource*, doi: 10.12686/SED-00000001-SHARE.

Harmsen, S., D. Perkins, and A. Frankel (1999). Deaggregation of probabilistic ground motions in the central and eastern United States, *Bull. Seismol. Soc. Am.* **89,** no. 1, 1–13.

Hough, S. (2014). Shaking from injection-induced earthquakes in the central and eastern United States, *Bull. Seismol. Soc. Am.* **104,** no. 5, 2619–2626.

Hunter, J. D. (2007). Matplotlib: A 2D graphics environment, *Comput. Sci. Eng.* **9,** no. 3, 90–95.

International Energy Agency Environmental Projects Ltd. (2013). Induced seismicity and its implications for CO2 storage risk, *Technical Report June*, International Energy Agency Environmental Projects Ltd. (IEAGHG), Cheltenham, United Kingdom.

Klose, C. D. (2013). Mechanical and statistical evidence of the causality of human-made mass shifts on the Earths upper crust and the occurrence of earthquakes, *J. Seismol.* 109–135, doi: 10.1007/s10950-012-9321-8.

Kostrov, V. V. (1974). Seismic moment and energy of earthquakes, and seismic flow of rocks, *Izvestiya Phys. Solid Earth* **1,** 23–44.

Majer, E., R. Baria, M. Stark, S. Oates, J. Bommer, and H. Asanuma (2007). Induced seismicity associated with enhanced geothermal systems, *Geothermics* **36,** no. 3, 185–222.

McGarr, A. (1976). Seismic moments and volume changes, *J. Geophys. Res.* **81,** no. 8, 1487–1494.

McGuire, R. K. (1995). Probabilistic seismic hazard analysis and design earthquakes: Closing the loop, *Bull. Seismol. Soc. Am.* **85,** no. 5, 1275–1284.

McGuire, R. K. (2008). Probabilistic seismic hazard analysis: Early history, *Earthq. Eng. Struct. Dynam.* **37,** 329–338.

Mena, B., S. Wiemer, and C. Bachmann (2013). Building robust models to forecast induced seismicity related to geothermal reservoir enhancement, *Bull. Seismol. Soc. Am.* **103,** no. 1, 383–393.

Mossop, A. (2012). An explanation for anomalous time dependent subsidence, in *46th US Rock Mechanics/Geomechanics Symposium*, Chicago, Illinois, 24–27 June, Vol. 12, 518.

Muntendam-Bos, A., and J. de Waal (2013). Reassessment of the probability of higher magnitude earthquakes in the Groningen gas field: Including a position statement by KNMI, *Technical Report January*, State Supervision of Mines.

Musson, R. M. W. (1999). Determination of design earthquakes in seismic hazard analysis through Monte Carlo simulation, *J. Earthq. Eng.* **3,** no. 4, 463–474, doi: 10.1080/13632469909350355.

Musson, R. M. W. (2000). The use of Monte Carlo simulations for seismic hazard assessment in the U.K., *Ann. Geofisc.* **43,** no. 1, 1–9.

National Academy of Sciences (2013). *Induced Seismicity Potential in Energy Technologies*, National Academy of Sciences, Washington, D.C.

Pagani, M., D. Monelli, G. Weatherill, L. Danciu, H. Crowley, V. Silva, P. Henshaw, L. Butler, M. Nastasi, L. Panzeri, *et al.* (2014). OpenQuake engine: An open hazard (and risk) software for the global earthquake model, *Seismol. Res. Lett.* **85,** no. 3, 692–702, doi: 10.1785/0220130087.

Parsons, T., S. Toda, R. Stein, A. Barka, and J. Dietrich (2000). Heightened odds of large earthquakes near Istanbul: An interaction-based probability calculation, *Science* **288,** 661–665.

Petersen, M., T. Cao, K. Campbell, and A. Frankel (2007). Time-independent and time-dependent seismic hazard assessment for the state of California: Uniform California earthquake rupture forecast model 1.0, *Seismol. Res. Lett.* **78,** no. 1, 99–109.

Petersen, M., M. Moschetti, P. Powers, C. S. Mueller, K. M. Haller, A. D. Frankel, Y. Zeng, S. Rezaeian, S. C. Harmsen, O. S. Boyd, *et al.* (2014). Documentation for the 2014 update of the United States national seismic hazard maps, *U.S. Geol. Surv. Open-File Rept. 2014-1091*, doi: 10.3133/ofr20141091.

Sharma, N., V. Convertito, N. Maercklin, and A. Zollo (2013). Ground-motion prediction equations for the Geysers geothermal area based on induced seismicity records, *Bull. Seismol. Soc. Am.* **103,** no. 1, 117–130.

Stauble, A. J., and G. Milius (1970). Geology of Groningen gas field, Netherlands, in *Geology of Giant Petroleum Fields*, M. Halbouty (Editor), American Association of Petroleum Geologists, Tulsa, Oklahoma, 359–369.

Strasser, F. O., N. A. Abrahamson, and J. J. Bommer (2009). Sigma: Issues, insights, and challenges, *Seismol. Res. Lett.* **80,** no. 1, 40–56, doi: 10.1785/gssrl.80.1.40.

Suckale, J. (2009). Chapter 2 – induced seismicity in hydrocarbon fields, *Adv. Geophys.* **51,** no. 09, 55–106, doi: 10.1016/S0065-2687(09)05107-3.

Wassing, B. B. T., T. Van Eck, and R. M. H. E. Van Eijs (2004). Seismisch hazard van genduceerde aardbevingen Integratie van deelstudies, *Technical Report, TNO NITG 04-244-B*, Utrecht, The Netherlands.

Shell Global Solutions International B.V.
Kessler Park 1
2288 GS Rijswijk
The Netherlands
S.J.Bourne@shell.com
(S.J.B., S.J.O.)

Civil and Environmental Engineering
Imperial College London
South Kensington Campus
London SW7 2AZ
United Kingdom
(J.J.B.)

Royal Netherlands Meteorological Institute (KNMI)
Utrechtseweg 297
3731GA De Bilt
The Netherlands
(B.D.)

Nederlandse Aardolie Maatschappij B.V. (NAM)
Schepersmaat 2
9405 TA Assen
The Netherlands
(J.v., D.D.)

Manuscript received 7 October 2014;
Published Online 19 May 2015